IEEE Photonics Journal
An IEEE Photonics Society Publication

Open Access

Electro-absorption and Electro-optic Characterization of L-Band InAs/InP Quantum-dash Waveguide

Volume 12, Number 3, June 2020

E. Alkhazraji
A. M. Ragheb
M. A. Esmail
Q. Tareq
H. Fathallah
S. A. Alshebeili
K. K. Qureshi
M. Z. M. Khan

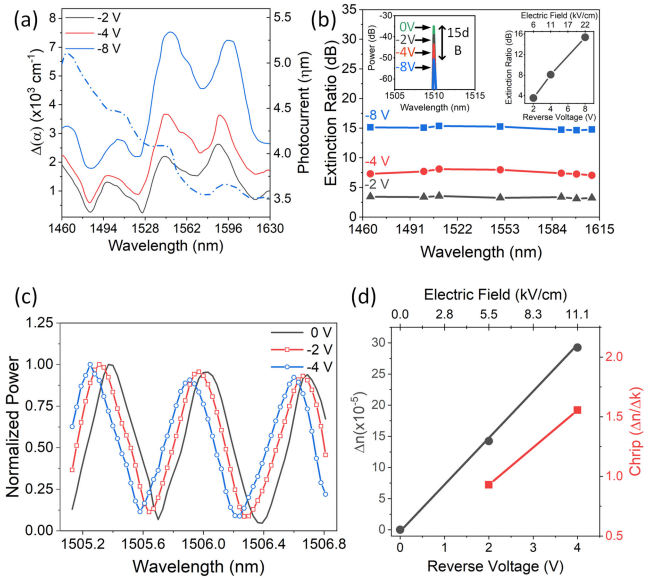

DOI: 10.1109/JPHOT.2020.2988584

Electro-absorption and Electro-optic Characterization of L-Band InAs/InP Quantum-dash Waveguide

E. Alkhazraji,[1,2] A. M. Ragheb,[3] M. A. Esmail,[4] Q. Tareq,[1] H. Fathallah,[5] S. A. Alshebeili,[3,6] K. K. Qureshi,[7] and M. Z. M. Khan[1]

[1]Optoelectronics Research Laboratory, Electrical Engineering Department, King Fahd University of Petroleum and Minerals (KFUPM), Dhahran 31261, Saudi Arabia
[2]Department of Electrical and Electronic Engineering Technology, Jubail Industrial College, Jubail 31961, Saudi Arabia
[3]KACST-TIC in Radio Frequency and Photonics for the e-Society (RFTONICS), King Saud University (KSU), Riyadh 11421, Saudi Arabia
[4]Communications and Networks Engineering Department, Prince Sultan University, Riyadh 11586, Saudi Arabia
[5]Computer Department, Faculty of Sciences of Bizerte, University of Carthage, Tunis 1054, Tunisia
[6]Electrical Engineering Department, King Saud University (KSU), Riyadh 11421, Saudi Arabia
[7]Electrical Engineering Department, King Fahd University of Petroleum and Minerals (KFUPM), Dhahran 31261, Saudi Arabia

DOI:10.1109/JPHOT.2020.2988584

Manuscript received January 27, 2020; revised April 13, 2020; accepted April 14, 2020. Date of publication April 20, 2020; date of current version May 26, 2020. The work of E. Alkhazraji, Q. Tareq, K. K. Qureshi, and M. Z. M. Khan was supported by Deanship of Research, King Fahd University of Petroleum and Minerals (KFUPM), under University Funded Grant IN171029. The work of A. M. Ragheb and S. A. Alshebeili was supported by King Saud University through the Researchers Supporting Project number (RSP-2019/46). Corresponding author: M. Z. M. Khan (e-mail: zahedmk@kfupm.edu.sa).

Abstract: Electro-absorption and electro-optic characteristics of InAs/InP quantum-dash active region-based waveguide, emitting at ∼1600 nm is investigated. Two major peaks were observed in the change of absorption spectrum with a maximum value of 7070 cm^{-1} at a bias voltage of -8V with an excellent uniform extinction ratio of ∼15 dB across the wavelength range of operation (1460–1620 nm). The effect of temperature on electro-absorption (EA) measurement suggests a strong influence resulting in merging of two major change of absorption spectrum peaks with higher temperature. Furthermore, electro-optic measurements indicate a change in refractive index and its efficiency values of $\sim 2.9 \times 10^{-4}$ and $\sim 0.5 \times 10^{-4}$ V^{-1}, respectively, hence exhibiting a low chirping factor of 0.9 and 1.5 at bias voltages of -2 V and -4 V, respectively. As a quasi-three-dimensionally confined structure possessing both quantum well- and quantum dot-like features, the quantum dash waveguide showed superior electro-absorption and electro-optic properties compared to quantum dots and close to that of quantum wells, while attaining low chirp and broad wavelength range of operation. This paves a way for potential realization of quantum dash-based EA and electro-optic modulator for future optical access networks, particularly operating in wide C- to L-band region.

Index Terms: Quantum-dash, quantum-dot, electro-absorption, electro-optic, modulators.

1. Introduction

In the recent years, self-assembled quantum dot (QDot) optical devices have piqued the interest of research and development owing to their three-dimensional quantum confinement that results in discretized zero-dimensional density of states and energy levels. This in turn, enables low threshold current densities, high optical powers, high efficiencies and differential gains to be realized in addition to temperature-insensitivity in optical sources and amplifiers. Consequently, most attention and effort in this field has been focused in employing these novel structures as optical sources, particularly mode-locked lasers, and optical amplifiers in optical fiber telecommunication systems [1]. Nevertheless, a very limited amount of work has been carried out in employing QDot-based structures as external modulators in the form of electro-absorption (EA) modulators (EAM) or electro-optic (EO) modulators (EOM) [2], which have been employed extensively in quantum-well (QWell) structures [3–6].

EAM and EOM are devices that are realized by exploiting the nonlinearity of optical materials as compact and efficient external modulators in telecommunication systems, in addition to enabling all-optical integration, laser-amplifier-modulator in particular [7]. QWell structures are characterized by a strong quantum confined stark effect (QCSE) near the exciton edge of absorption, which in turn, results in a built-in birefringence, high EA extinction ratios (ERs), in addition to high EO coefficients and Kerr effects, thus making them highly preferred quantum confined nanostructures for EAMs and EOMs [14]. On the other hand, at first glance QDot structures should show similar excellent EO and EA characteristics due to the enhanced stark effect and steep edge of absorption in addition to the high degree of optical non-linearities compared to bulk materials [8]. However, in reality, they are back-drawn by the decoupled nature between the gain and reservoir which is very beneficial to mode-locked lasers and optical amplifiers. Nonetheless, this hinders the performance of the structure as a modulator since the depletion of the carriers necessitates scattering out the large energy spacing carriers prior to the depletion of the carrier density, and also reduces the excitonic effects and results in their absence in the absorption spectra. [15]. Indeed, different reports in literature show that QDot structures are inferior EAMs and EOMs in terms of EO coefficients and EA extinction ratios. On the other hand, QDots offer an extra advantage of broad range of operation wavelength due to their inhomogeneous growth nature, compared to QWell devices where these effects are limited to narrow spectral ranges around the bandgap energies.

Table 1 summarizes different reports on QDot- and QWell-based waveguides as EAMs and EOMs alongside their respective EO or EA characteristics. Indisputably, QWell structures have shown superior EA characteristics over the QDots counterpart. For instance, a 17 dB (10 dB) ER was achieved over a multiple-QWell InGaAsP/InP structure emitting around 1540 nm while biased at -3 V (-2 V) [3] ([4]). Subsequently, an ER of 12 dB was achieved at a mere bias voltage of -1.2 V over the same structure, thus showing effective exploitation of the enhanced QCSE from QWell structures [5]. Conversely, low ERs of 2.1 and 3.5 dB were reported on InAs and InGaAs QDot structures, respectively, in [7] and [8], emitting around 1300 nm even when biased at high reverse bias voltage of -10 V in the former case. Recently, an improved performance from an InAs (InGaAs) QDot waveguide was reported in [2] ([9]) exhibiting an ER of 10 dB (10.5 dB) at 1300 nm when biased at -8 V. Moreover, in order to improve the device characteristics, a thin GaP tensile strain compensation layer between the different QDot layers was incorporated [10], with the demonstration of the best ER of 13 dB at – 8 V, to the authors' knowledge, over the QDot platform. However, this was only possible to be achieved at the cost of ten QDot layers.

In terms of the EO characteristics, a similar outline can be observed from Table 1 between QWell and QDot devices. For instance, a change in the refractive index (Δn) as high as 1.5×10^{-3} was reported over a InGaAsP/InP three-step QWell structure emitting around 1500 nm with a corresponding efficiency $\Delta n/\Delta V$ of 2.8×10^{-4} V^{-1} [6]. On the other hand, the InAs/GaAs QDot structure in [11] ([12]) showed a Δn value of 1.3×10^{-4} (2.0×10^{-4}) around $\sim$1500 nm with corresponding $\Delta n/\Delta V$ of 0.33×10^{-4} V^{-1}. Moreover, from a modified InGaAs QDot structure (stacks of QDots connected by quantum wires), $\Delta n = 0.8 \times 10^{-4}$ was demonstrated at 1500 nm with $\Delta n/\Delta V = 0.1 \times 10^{-4}$ V^{-1} [13].

TABLE 1
Summary of the Reported EO and EA Characteristics on QDot and QWell Waveguides in Literature, Compared to the QDash Waveguide Investigated in This Work

Quantum structure	Material system	λ (nm)	ER @ V_A^* (dB)	Δn	$\Delta n/\Delta V^{**}$ (V^{-1})	Ref.
QDot	InAs/GaAs	1300	10 @-8V	-	-	[2]
	InAs/InGaAs	1300	2.1 @-10V	-	-	[7]
	InGaAs/GaAs	1300	3.5 @-10V	-	-	[8]
	InGaAs/GaAs	1300	10.5 @-8V	-	-	[9]
	InAs/GaAs	1300	13 @-8V	-	-	[10]
	InAs/GaAs	1500	-	1.3×10^{-4}	0.33×10^{-4}	[11]
	InAs/GaAs	1500	-	2×10^{-4}		[12]
	InGaAs/GaAs	1500	-	0.8×10^{-4}	0.1×10^{-4}	[13]
QDash	InAs/InP	1600	15 @-8V	2.9×10^{-4}	0.5×10^{-4}	This Work
QWell	InGaAsP/InP	1540	10 @-2V	-	-	[3]
	InGaAsP/InP	1550	17 @-3V	-	-	[4]
	InGaAsP/InP	1550	12 @-1.2 V	-	-	[5]
	InGaAsP/InP	1500	-	1.5×10^{-3}	2.8×10^{-4}	[6]

*V_A is the applied reverse voltage to bias the waveguide.
**$\Delta n/\Delta V$ is the rate of refractive index change per Volt.

Recently, a new class of quantum confined nanostructures, namely quantum dash (QDash), which has quasi-three-dimensional confinement features, has emerged as a strong contender for C- and L-band optical communications [16]. These InAs/InP QDash structures possess niche characteristics in between QWell and QDot counterparts, besides exhibiting wide wavelength emission tunability [17] and broadband wavelength characteristics owing to their inhomogeneous growth process. In fact, several reports on employing QDash active region in lasers and amplifiers encompassing 1500 to 1700 nm have affirmed QDot- and quantum wire (QWire)-like performance characteristics [18]. In particular, broadband lasing emission from this nanostructure is very appealing in optical communications, specifically in the mid and far L-band (∼1600–1625 nm) region that is under consideration for future optical networks. Hence, in this work, we comprehensively investigated both EA and EO characteristics of an InAs/InP QDash structure emitting at ∼1600 nm, and showing superior properties over QDot counterpart, in terms of 15 dB ER at −8V, Δn with its corresponding efficiency $\Delta n/\Delta V$ of 0.5×10^{-4}. In other words, QDashes combine benefits of low chirp of QDots while at the same time demonstrate much better extinction ratio close to QWells. Acquiring these features, in addition to wide wavelength operation (∼1460–1615 nm) covering S-, C- and L-band makes InAs/InP QDash based EAM or EOM devices highly attractive and promising unified modulators in future optical networks that are considering extending the optical communication window beyond C-band to the adjacent bands. To the best of our knowledge, this is the first demonstration of InAs/InP QDash waveguide EA and EO characteristics as well as the proposal of employing QDash modulator devices for wide wavelength operation in optical communications unlike QWell counterparts that are typically narrow wavelength band devices.

2. Experimental Setup

The investigation in this work is carried out over a bare $3 \times 500\ \mu m^2$ L-band quantum dash-in-a-well ridge-waveguide (QD-WG). The self-organized InAs/InP QDash device chirped barrier thickness structure was grown by molecular beam epitaxy on a (100) oriented S-doped n-type InP substrate. Fig. 1(a) illustrates the epitaxy structure of the QD-WG whose active region is consisted of four 5-ML thick InAs dash layers each embedded within 7.6 nm thick compressively strained $In_{0.64}Ga_{0.16}Al_{0.2}As$ QWells. Each stack is topped by a tensile-strained $In_{0.50}Ga_{0.32}Al_{0.18}As$ top barrier layer. The structure was chirped by varying the thickness of each top barrier layer, *viz.* 10,10,15, and 20 nm, in order to increase the inhomogeneity of the structure and achieve a broader

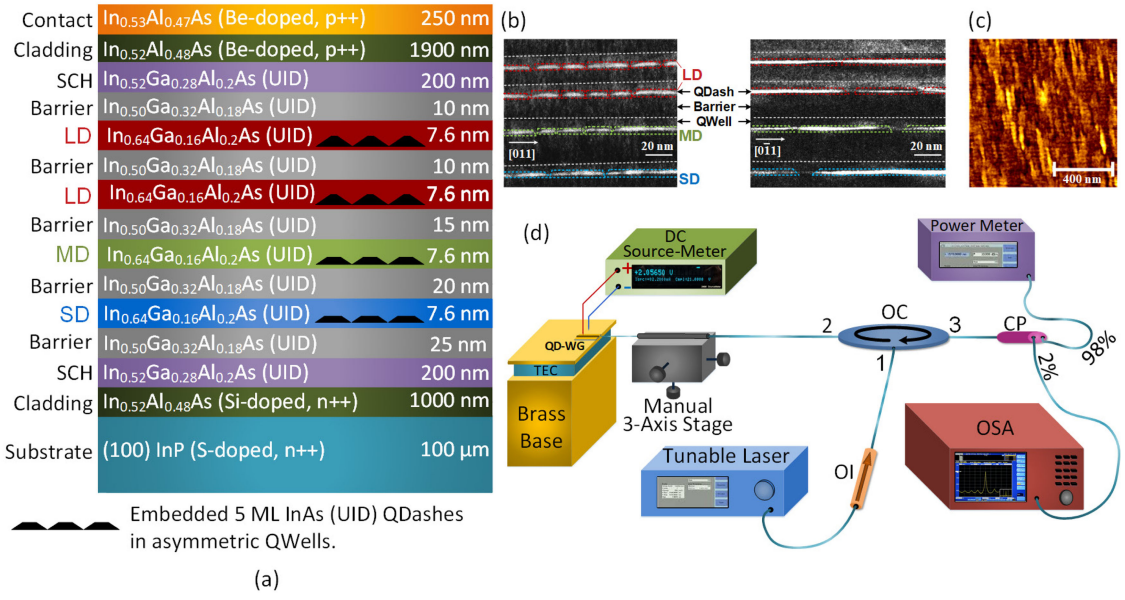

Fig. 1. (a) Epitaxy structure of the QD-WG structure and the corresponding (b) TEM micrographs along [011] and [01̄1] directions. (c) AFM image of the QDashes revealing the in-plane size dispersion. (d) Block diagram of the experimental setup utilized for electro-absorption and electro-optics characterization of the QD-WG.

gain profile. This is a result to the fact that the barrier layer thickness plays a vital role in determining the size, height in particular, of the grown subsequent dashes, and hence their corresponding ground state (GS) transition energies. In general, thinner barrier layer thickness results in grown dashes of larger average-height, which in turn are associated with smaller GS transition energies (*i.e.*, shorter wavelengths), and vice versa [19]. In order to facilitate discussion in the subsequent section, different QDash stacks are designated here according to their sizes as: large dash (LD) group corresponding to the overgrown dashes of the two 10-nm barriers, in addition to medium dash (MD) and small dash (SD) ensembles of the 15- and 20-nm barriers, respectively. It is to be noted that due to the high possibility of coupling between the top two QDash stacks (10 nm barrier thickness) in addition to their overlapped density of states (DoS) [20], a collective single LD group is considered [21]. Fig. 1(b) shows cross-sectional transmission electron microscopic (TEM) micrographs of the QD-WG's active region along [011] and $0\bar{1}1$ directions wherein the QDashes (bright structures) in asymmetric QWell is evident. The TEM images reflect an estimated QDash average length and width of $\sim$100 and $\sim$18 nm, respectively, while the average dash-height is $\sim 3.0 \pm 0.5$, $\sim 2.7 \pm 0.5$ and $\sim 2.5 \pm 0.5$ nm for the LD, MD, and SD ensembles [18]. On the other hand, Fig. 1(c) depicts an atomic force microscopic (AFM) image of the QDashes exhibiting highly inhomogeneous sizes composed of a mixture between quantum wire-like and QDot-like features. The density of the QDashes is estimated as $\sim 5 \times 10^{10}$ cm^{-2} with a coverage of $\sim$70%.

The experimental setup employed to investigate the EA and EO characteristics of the QD-WG is shown in Fig. 1(d). The bare QD-WG with as-cleaved facets was mounted over a custom-made brass base with a thermoelectric cooler (TEC) assembly. The single facet output power of the QD-WG was butt coupled into a lensed SMF ($\sim$5% or -13 dB coupling efficiency) via a manual 3-axis translation stage passing into port 2 of an optical circulator (OC). Moreover, a tunable laser (TL) was passed into port 1 of the OC through an optical isolator (OI). The OC injects the emission of the TL into the cavity of the QD-WG through one butt-coupled facet. Thereafter, after travelling through the whole cavity of the QD-WG, the emission reflects off the other facet and travels back to be ejected out into the coupled SMF. In the meantime, a reverse-bias DC voltage was exerted across

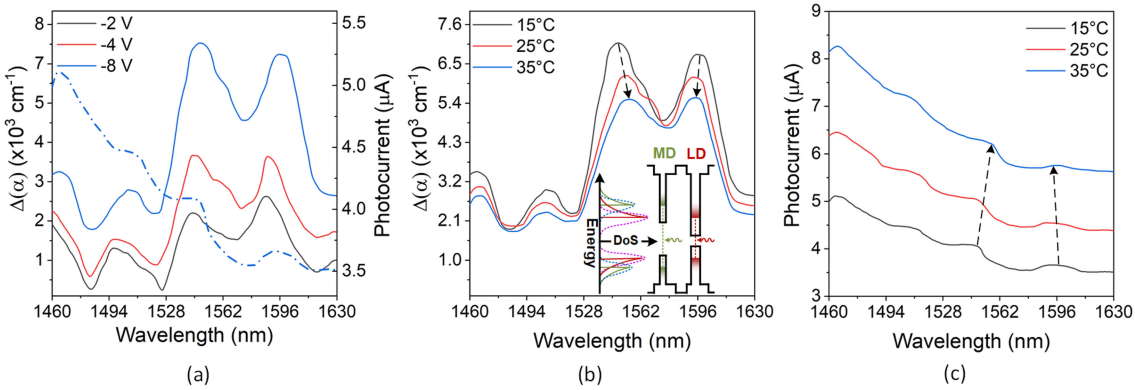

Fig. 2. (a) The measured change in absorption under different applied reverse bias voltages in addition to the measured photocurrent (dashed line) at a bias voltage of −8 V as functions of wavelength at a fixed temperature of 15 °C, (b) The measured change in absorption, and (c) photocurrent under a fixed bias voltage of −8 V for different temperatures. The inset of (b) shows a qualitative transition energy band diagram of the InAs/InP QDash waveguide active region along with the Gaussian distributed DoS.

the QD-WG via a DC source-meter (Keithley 2400) to induce an electric field perpendicular to the quantum dash layers of the structure altering its overall absorption (and transmission) coefficients. Furthermore, the DC source-meter was utilized additionally to measure the collected photocurrent that results from photon absorption in the structure. At each applied reverse bias voltage, the entire transmitted emission through the QD-WG from port 2 to port 3 of the OC was split via a 2:98% optical coupler (CP) into an optical spectrum analyzer (OSA) with a 60-pm resolution and an optical power meter, respectively.

3. Measurements Results and Discussion

We firstly started by analyzing the EA of the QD-WG at a fixed temperature. Thereafter, the temperature effects on the EA characteristics are investigated. Finally, we explore the EO characteristics of the devices as a potential EOM.

3.1 Electro-absorption characteristics

To obtain the EA characteristics of the device, the TL was swept between 1460–1630 nm covering the whole S-, C-, and L-bands. Meanwhile, the electro-transmission measurements were carried out under different applied reverse-bias voltages across the QD-WG where the transmitted power was measured at each point to obtain the transmission spectrum profile of the structure. Thereafter, the spectrum of the change in absorption ($\Delta\alpha$) with respect to the transmission at zero bias voltage was derived according to [22]:

$$\Delta\alpha = -\frac{1}{d} ln\left(\frac{P_V}{P_0}\right) \tag{1}$$

where d is the total thickness of the active region, P_V is the transmitted optical power under a given reverse bias voltage, and P_0 refers to the optical power at zero bias voltage. The absorption changes induced by the applied external field take place for photon energies near the transition energy of quantum dashes within the space charge region of the p−i−n junction. As such, Fig. 2(a) shows the obtained $\Delta\alpha$ spectrum for reverse bias voltages of −2, −4, and −8 V under a fixed temperature of 15 °C. At first glance, two major peaks appear in the $\Delta\alpha$ spectrum around ∼1545, and ∼1590 nm. In addition, very minor peaks are observed around ∼1460, ∼1500 nm, which are ascribed to the SD group and the fringe dashes at the extreme tails of the SD and MD dash size distributions. These

two major peaks at short (long) wavelengths are attributed to the dominant absorption from the average size QDashes of MD (LD) ensembles corresponding to mean larger (smaller) GS transition energies with most available DoS (larger active volume compared to SD group). Nevertheless, with higher applied voltages, the absorption peaks witnessed a slight redshift in addition to a broadening effect indicating that the applied field results in shifting the photons to lower energies. In particular, the major two peaks of MD and LD ensembles at -2V shifted from 1543 and 1587 nm, to 1548 and 1598 nm, respectively, as the applied reverse bias voltage was increased to -8 V, while $\Delta\alpha$ increased from $\sim$2320 cm^{-1} to $\sim$7070 cm^{-1} between the two voltage points for the 1543-nm peak.

Moreover, the dashed curve in Fig. 2(a) depicts the measured photocurrent for the -8 V case as a function of wavelength wherein four distinct humps can be observed corroborating well with the wavelengths of the peaks of the $\Delta\alpha$ spectrum since maximum absorption takes place at these peaks resulting in a surge in the collected photocurrent represented by these humps. In our previous work [21], only two peaks were shown for this structure's absorption spectrum, measured by from segment-contact method, which at a first glance seemed to be not in compliance with our measurements here. Nevertheless, after close inspection, we attributed that junction heating due to direct current operation played a significant role in changing the absorption profile. To ascertain this, we obtained the $\Delta\alpha$ spectra under a fixed bias voltage of -8 V at different temperatures, namely 15, 25, and 35 °C, which are plotted in Fig. 2(b). Indeed, increasing the temperature resulted in red-shifting the first major peak (*i.e.*, of MD group) while blue-shifting the second one (*i.e.*, of LD ensemble). Interestingly, this indicates the eventual gradual merging between these peaks into a single peak around $\sim$1580–1585 nm. Moreover, an overall reduction in $\Delta\alpha$ is observed throughout the whole spectrum. This evolution is depicted in Fig. 2(b)–(c) by the dashed arrows. This suggests that the higher junction temperature assists in increasing the absorption of the zero-bias reference case (α_0) resulting in shrinking $\Delta\alpha$ with applied voltage. To further affirm this observation, Fig. 2(c) shows the corresponding measured photocurrents whose humps also witnessed identical blue- and red-shifting action when the temperature is increased from 15 to 35 °C. More importantly, increasing the temperature showed higher photocurrent levels indicating that the -8 V absorption spectrum (α_V) is high though $\Delta\alpha$ becomes smaller since α_0 has also increased with elevated junction temperature.

This could be qualitatively explained by referring to the transition band energy diagram of the QDash waveguide active region illustrated in the inset of Fig. 2(b) and the corresponding Gaussian inhomogeneously distributed QDash transition energies states of respective ensembles due to self-assembled growth process. Elevated temperature assists in a more uniform distribution of carriers across the QDash active region via various carrier movement mechanisms (carrier leakage/spillover, direct as well as phonon assisted tunneling, etc.) [23, 24], which is highly possible in an inhomogeneous system, thus enabling more QDashes of MD and LD groups to participate in the absorption process. In other words, in-plane coupling (*i.e.*, within a QDash group) as well as coupling across the MD and LD groups are promoted at higher temperatures, thanks to the junction temperature rise. In this scenario, the relatively larger (smaller) QDashes of MD (LD) group, exhibiting comparatively shorter (higher) GS transition energy, with highly overlapping Gaussian distributed DoS, could compete and possibly dominate the absorption process with the availability of more carriers to participate. This results in red (blue) shifting of the absorption peaks. On the other hand, the absorption of fringe smaller (larger) QDashes, corresponding to higher (shorter) transition energies of the MD (LD) group, may saturate or fade with increasing temperature due to fewer Gaussian distributed DoS (*i.e.*, at its tail) and availability of carriers. Hence, these processes assist in red (blue) shifting the MD (LD) group absorption peaks with increasing temperature and finally couple into a single peak indicating highly coupled MD and LD ensembles. It is to be noted that temperature dependent QDash transition energy shrinkage (*i.e.*, red shifting of absorption peak) would also affect both of these major absorption peaks, however, Fig. 2(b) indicates that the qualitative model discussed above ultimately dominates. Furthermore, it is noteworthy to mention here that uniform carrier distribution among the Qdashes could also possibly explain the exhibited broadened absorption peaks as well as their reduced $\Delta\alpha$ values as the carriers are now more

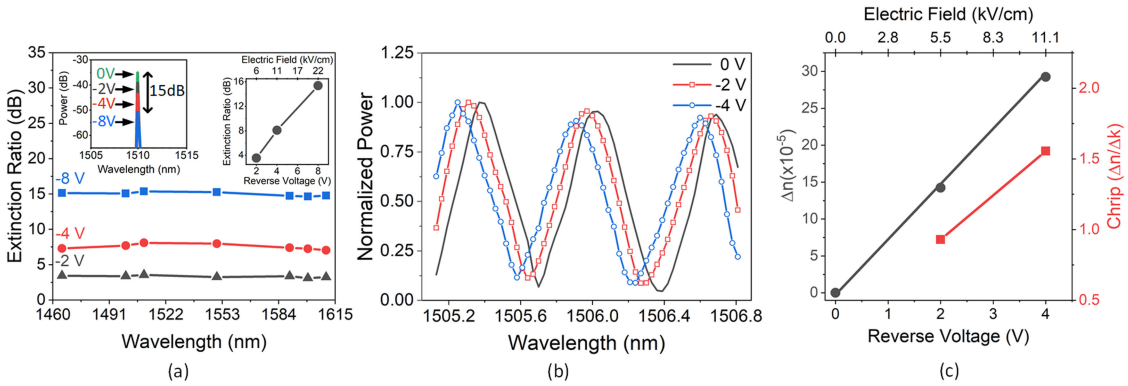

Fig. 3. (a) The obtained extinction ratio at different wavelengths under applied voltages of −2, −4, and −8 V. The left inset shows the measured spectrum of the TL tuned at ∼1510 nm after being transmitted through the QD-WG while being biased with different voltages. The right inset depicts the extinction ratio for the same wavelength for the different applied voltages. (b) The FP resonance shift exhibited as the reverse bias voltage is changed from 0 to −4 V. (c) The extracted change in refractive index and chirp factor as functions of the applied reverse voltage.

spread across different size Qdashes of the ensembles rather than being concentrated in certain Qdashes, which was the case at lower temperatures.

To further demonstrate the potential of utilizing this structure as an EAM, the ER was obtained for applied reverse voltages of −2, −4, and −8 V, and are shown in Fig. 3(a) for different wavelengths across the whole window of investigation. This was carried out by measuring the lasing spectra of the transmitted emission of the TL through the QD-WG's cavity under different applied reverse bias voltages. For instance, the left inset of Fig. 3(a) shows the transmitted emission spectra when the TL was tuned to ∼1510 nm at 15 °C under applied reverse bias voltages of −2, −4, and −8 V alongside the unbiased case (0 V). A maximum ER of ∼15 dB was obtained under an applied voltage of −8 V with respect to the unbiased case while the −2 and −4 V cases showed ERs of ∼3.5 and ∼7.5 dB, respectively. The right inset of Fig. 3(a) depicts the ER at ∼1510 nm as a function of the applied reverse bias voltage and electric field and exhibiting a near-linear relation. Furthermore, Fig. 3(a) shows a very minimal variation (±0.5 dB) in the measured ERs throughout the whole window of investigation (∼1460–1615 nm) demonstrating the potential broadband wavelength operation, besides exhibiting robustness and flexibility of employing this structure in EA modulation with uniform performance independently of the wavelength.

When compared to previous reports in literature, as summarized in Table 1, the QD-WG under investigation shows better results than QDot structures. For instance, The InGaAs/GaAs QDot device that was reported [9] showed the best ER 10.5 dB at 1300 nm when biased at −8 V compared to the ∼15 dB ratio, which is obtained from QD-WD at the same applied voltage. Nevertheless, QWell structures have shown superior EA characteristics when compared to the QDash structure under test here. For instance, a 17-dB ER was achieved over a multiple-QWell InGaAsP/InP structure emitting around 1540 nm while biased at −3 V [3]. This can be explained by the weaker confinement of QDash structures, and the corresponding localization of the wavefunction, which results in a greater shift in the edge of absorption under applied electric fields compared to QDots, yet still lower than QWells. QDots typically are associated with much lower overlap/confinement factors (Γ) compared to QWell structures due to their higher degree of quantum confinement, which in turn, limits the effective absorption ($\alpha_{eff} = \Gamma\alpha$) since larger portions of the light travels and transmits outside of the active region's boundaries. More significantly, QDots have been shown to exhibit a much weaker (linear) dependence of the QCSE edge-of-absorption shift on the applied electric field when compared to the quadratic relationship in the case of QWells [1, 25]. QDashes on the other hand, possess higher Γ compared to QDots, yet lower than QWells, due to their

weaker quantum-confinement lying between QDots and QWells. For instance, the multiple-layer QDot structure in [11] showed a very low $\Gamma = 0.01$ whearas the QD-WG has $\Gamma = 0.03$. Higher Γ values of QDash structures allow more absorption to take place as the light beam propagates through the waveguide of larger active region volume compared to QDot counterparts, with the application of electric field. Moreover, the probability of photon assisted tunneling also increases in the QDash case, thus assisting in an increased absorption [23, 24, 26]. This explains why adding the ten QDot layers in [10] improved the EA performance as it increased Γ, and ultimately the absorption of the structure, in addition to increasing the probability of photon assisted tunneling and absorption instances to take place. In addition, having multiple layers increases the aggregate dependence of the QCSE on the applied electric field [25]. Hence, the QDash structure under test here shows a great potential as an EAM, thanks to the superior EA characteristics to QDots. In other words, QDash as an EAM could provide high ERs similar to that of QWell structures while, simultaneously, providing the broad wavelength range of operation feature of QDots.

3.2 Electro-optic characteristics

Next, EO measurements were also conducted on the same structure to explore its properties in EO modulation. To that end, the voltage-dependent shift of the Fabry-Perot (FP) resonances exhibited by the structure under different bias voltages was measured and is depicted in Fig. 3(b). This measurement was performed by finely sweeping the emission of the TL (30-pm step size) over a 1.68-nm window near ∼1505 nm, while measuring the detected power at each step. Fig. 3(b) shows a FP blue shift of 68 pm and 131 pm at a reverse bias voltage of −2 V and −4, respectively, compared to the 0 V bias case. Thereafter, the well-known FP transmission equation was used to extract the refractive index (n) of the QD-WG, given by [27]:

$$P_{out} = P_{in} \frac{(1-R)^2 e^{-\alpha_i L}}{\left(1 - Re^{-\alpha_i L}\right)^2 + 4Re^{-\alpha_i L}\sin^2\left(\frac{2\pi nL}{\lambda}\right)} \tag{2}$$

where P_{out} and P_{in} are the output and input powers through the cavity, respectively, R is the mirror reflectivity of the laser cavity, α_i is the loss coefficient of the structure, L is the cavity length, and λ is the wavelength. It is worth mentioning here that double the cavity length was used here for L in order to account for the round trip of the injected and reflected beam. As such, n was solved for in (2) under each applied reverse bias voltage, and thereafter Δn was calculated with reference to the 0 V bias case. The obtained Δn value is shown in Fig. 3(c) as a function of both the applied reverse bias voltage and corresponding electric field. A maximum refractive index change of $\Delta n = 2.9 \times 10^{-4}$ was obtained at 4 V (11.1 kV/cm) with a $\Delta n/\Delta V = \sim 0.5 \times 10^{-4}$ V^{-1}. This value is higher than QDot structures operating at the same wavelength window and operating conditions of −4 V, which showed a $\Delta n = 1.3 \times 10^{-4}$ around ∼1500 nm with a $\Delta n/\Delta V$ of 0.33×10^{-4} V^{-1}. On the other hand, QWell based structures have again shown higher Δn values and $\Delta n/\Delta V$ rates compared to the QDash structure. For example, a Δn as high as 1.5×10^{-3} was reported over an InGaAsP/InP three-step QWell structure emitting around 1500 nm with a $\Delta n/\Delta V$ of 2.8×10^{-4} V^{-1} [6].

Another important parameter for an EOM is the chirp factor $\Delta n/\Delta k = 4\pi\Delta n/\lambda\Delta\alpha$ that is expected to be low as it ensures high contrast ratios in EOMs (for instance Mach–Zehnder modulators (MZM) [6]) thereby enabling high-data rate communication. Hence, $\Delta n/\Delta k$ for the QDash structure was also extracted from the measured Δn and $\Delta\alpha$ values and is shown in Fig. 3(c). This value is found to be 0.9 and 1.5 at −2 V and −4 V, respectively, which complies with the low chirp factors of QWell structures such as the ∼1.1 chirp factor that was reported over the QWell-based EAM integrated with a distributed feedback (DFB) laser in [28]. Hence, this analysis suggests that the QDash structure's EO characteristics again remain in between QDots and QWells in terms of performance. This comprehensive investigation of EA and EO characteristics of QDash further affirms the quasi-zero-dimensional DoS feature with performance in between QDot and QWire nanostructures that we have proposed before [18].

4. Conclusion

We investigated both the EA and EO characteristics of a chirped multi-stack broadband InAs/InP QDash structure. The EA characteristics initially showed two major peaks of change in the absorption coefficient around 1545, and 1590 nm. However, with increased temperature, the longest two peaks started to gradually shift and merge into a single peak around 1580 nm. The device has shown great EA characteristics in the form of a high extinction ratio of ($\sim$15 dB) at a drive voltage of -8 V consistently across a broad wavelength range (1460–1620 nm). We also analyzed the EO characteristics of the structure; In terms of the change of refractive index and its efficiency, the device demonstrated $\Delta n = 2.9 \times 10^{-4}$ at -4 V (11.1 kV/cm) with a $\Delta n/\Delta V = \sim 0.5 \times 10^{-4}$ V^{-1}. In other words, the QD-WG combines advantages showed by QWell (excellent EO and EA characteristics) and QDot (ultra-broad range of operation) structures. Furthermore, the device also showed a low chirping factor of 0.9 and 1.5 at -2 V and -4 V, respectively. These results show the potential of utilizing the structure as both an EAM and an EOM with excellent performance in unified next generation passive optical network (NG-PON) infrastructures.

References

[1] C. Ngo *et al.*, "Investigation of semiconductor quantum dots for waveguide electroabsorption modulator," *Nanoscale Research Letters*, vol. 3, no. 12, p. 486, Oct. 2008.

[2] S. Y. Lee, S. F. Yoon, A. C. Y. Ngo, and T. Guo, "Effects of annealing on performances of 1.3-μm InAs-InGaAs-GaAs quantum dot electroabsorption modulators," *Nanoscale Research Letters*, vol. 8, no. 1, p. 59, Feb. 2013.

[3] F. Devaux *et al.*, "InGaAsP/InGaAsP Multiple-Quantum- Well Modulator with Improved Saturation Intensity and Bandwidth Over 20 GHz," *IEEE Photonics Technology Letters*, vol. 4, no. 7, pp. 720–723, Jul. 1992.

[4] F. Devaux, E. Bigan, B. Rose, M. Mckee, F. Huet, and M. Carre, "High-speed InGaAsP/InP multiple quantum well, 1.55 μm singlemode modulator," *Electronics Letters*, vol. 27, no. 21, pp. 1926–1927, Oct. 1991.

[5] F. Devaux *et al.*, "20 Gbit/s operation of a high-efficiency InGaAsP/InGaAsP MQW electroabsorption modulator with 1.2-V drive voltage," *IEEE Photonics Technology Letters*, vol. 5, no. 11, pp. 1288–1290, Nov. 1993.

[6] H. Mohseni, H. An, Z. A. Shellenbarger, M. H. Kwakernaak, and J. H. Abeles, "Enhanced electro-optic effect in GaInAsP–InP three-step quantum wells," *Applied Physics Letters*, vol. 84, no. 11, pp. 1823–1825, March 2004.

[7] D. B. Malins, A. Gomez-Iglesias, E. U. Rafailov, W. Sibbett, and A. Miller, "Electroabsorption and Electrorefraction in an InAs Quantum-Dot Waveguide Modulator," *IEEE Photonics Technology Letters*, vol. 19, no. 15, pp. 1118–1120, Jul. 2007.

[8] C. Lin *et al.*, "InGaAs self-assembly quantum-dot monolithic integration of Semiconductor optical amplifier and electroabsorption modulator," in *2010 23rd Annual Meeting of the IEEE Photonics Society*, pp. 285–286, Nov. 2010 2010.

[9] Y. Chu, M. G. Thompson, R. V. Penty, I. H. White, and A. R. Kovsh, "1.3 μm quantum-dot electro-absorption modulator," in 2007 *Conference on Lasers and Electro-Optics (CLEO)*, pp. 1–2, May 2007 2007.

[10] C. Y. Ngo *et al.*, "Electroabsorption Characteristics of Single-Mode 1.3-μm InAs–InGaAs–GaAs Ten-Layer Quantum-Dot Waveguide," *IEEE Photonics Technology Letters*, vol. 22, no. 23, pp. 1717–1719, Dec. 2010.

[11] I. B. Akca *et al.*, "Electro-optic and electro-absorption characterization of InAs quantum dot waveguides," *Opt. Express*, vol. 16, no. 5, pp. 3439–3444, Mar. 2008.

[12] G. Moreau *et al.*, "Enhanced In(Ga)As/GaAs quantum dot based electro-optic modulation at 1.55 μm," *Applied Physics Letters*, vol. 91, no. 9, p. 091118, Aug. 2007.

[13] J. Shin, H. Kim, P. M. Petroff, and N. Dagli, "Enhanced Electro-Optic Phase Modulation in InGaAs Quantum Posts at 1500 nm," *IEEE Journal of Quantum Electronics*, vol. 46, no. 7, pp. 1127–1131, Apr. 2010.

[14] R. B. Welstand, S. A. Pappert, C. K. Sun, J. T. Zhu, Y. Z. Liu, and P. K. L. Yu, "Dual-function electroabsorption waveguide modulator/detector for optoelectronic transceiver applications," *IEEE Photonics Technology Letters*, vol. 8, no. 11, pp. 1540–1542, Nov. 1996.

[15] J. C. Norman, D. Jung, Y. Wan, and J. E. Bowers, "Perspective: The future of quantum dot photonic integrated circuits," *APL Photonics*, vol. 3, no. 3, p. 030901, Feb. 2018.

[16] M. A. Shemis *et al.*, "Broadly Tunable Self-injection Locked InAs/InP Quantum-dash Laser Based Fiber/FSO/Hybrid Fiber-FSO Communication at 1610 nm," *IEEE Photonics Journal*, vol. 10, no. 2, pp. 1–10, Feb. 2017.

[17] M. Z. M. Khan, T. K. Ng, and B. S. Ooi, "Self-assembled InAs/InP quantum dots and quantum dashes: Material structures and devices," *Progress in Quantum Electronics*, vol. 38, no. 6, pp. 237–313, Nov. 2014.

[18] M. Z. M. Khan, T. K. Ng, C.-S. Lee, P. Bhattacharya, and B. S. Ooi, "Chirped InAs/InP quantum-dash laser with enhanced broad spectrum of stimulated emission," *Applied Physics Letters*, vol. 102, no. 9, p. 091102, Mar. 2013.

[19] J. X. Chen *et al.*, "Tuning InAs/GaAs quantum dot properties under Stranski-Krastanov growth mode for 1.3 μm applications," *ACS Photonics*, vol. 91, no. 10, pp. 6710–6716, 2002.

[20] P. Miska *et al.*, "Vertical electronic coupling between InAs/InP quantum-dot layers emitting in the near-infrared range," vol. 86, no. 11, p. 111905, Mar. 2007.

[21] M. Z. M. Khan, M. A. Majid, T. K. Ng, D. Cha, and B. S. Ooi, "Simultaneous quantum dash-well emission in a chirped dash-in-well superluminescent diode with spectral bandwidth $>$700 nm," *Opt. Lett.*, vol. 38, no. 19, pp. 3720–3723, Oct. 2013.

[22] C. Shen *et al.*, "High-Modulation-Efficiency, Integrated Waveguide Modulator–Laser Diode at 448 nm," *ACS Photonics*, vol. 3, no. 2, pp. 262–268, Feb. 2016.
[23] W. Jaskólski, M. Zielinski, and G. W. Bryant, "Coupling and strain effects in vertically stacked double InAs/GaAs quantum dots: Tight-binding approach," *Acta Physica Polonica-Series A General Physics*, vol. 106, no. 2, pp. 193–206.
[24] C. Y. Jin *et al.*, "Effects of photon and thermal coupling mechanisms on the characteristics of self-assembled InAs/GaAs quantum dot lasers," *Physical Review B*, vol. 76, no. 8, p. 085315, Aug. 2007.
[25] S. Sobhani *et al.*, "Study of electro-absorption effects in 1300nm In(Ga)As/GaAs quantum dot materials," in *Physics and Simulation of Optoelectronic Devices XXIV (SPIE OPTO)*, vol. 9742, p. 97420S, California, USA, Mar. 2016.
[26] M. Fukuda, *Optical semiconductor devices*. John Wiley & Sons, 1998.
[27] A. Yariv and P. Yeh, *Photonics: Optical Electronics in Modern Communications*, 6 ed. New York, USA: Oxford University Press, 2006.
[28] W. Kobayashi *et al.*, "Design and Fabrication of 10-/40-Gb/s, Uncooled Electroabsorption Modulator Integrated DFB Laser With Butt-Joint Structure," *Journal of Lightwave Technology*, vol. 28, no. 1, pp. 164–171, Jan. 2010.